



Scheme 1 (A) Mechanism of heptamethine Cy7 for the ratiometric fluorescence imaging of HClO.²³ (B) Structures of probes ClO1–ClO6.

Results and discussion

In this study, we aim to design lung-targeting probes and detect HClO molecules in the event of inflammation. To date, numerous studies have explored lipid and polymer based nanoparticles for the delivery of therapeutic cargo to the lungs.^{39–42} For example, researchers employed cationic or ionizable lipids to deliver DNA or siRNA to the lungs of mice.^{40,42} Based on these studies, we speculate that lipid chains and amino groups may contribute to the accumulation of delivery materials along with their cargo in the lungs. Therefore, we conceived a series of heptamethine Cy7 based cyanine derivatives, ClO1–ClO6, as fluorescent ratiometric HClO probes (Scheme 1B). According to the methods reported previously,²³ ClO1–ClO6 were synthesized through two-step reactions. The synthetic routes to ClO1–ClO6 are described in the ESI.† The structures of ClO1–ClO6 were confirmed by ¹H NMR and high-resolution mass spectrometry (ESI†). To confirm the mechanism shown in Scheme 1, we treated ClO1 with HClO and measured the resulting product through mass spectra. A new

peak of $m/z +16$ was found (ESI, Fig. S1†), which corresponds to the epoxides produced by the oxidation of the double bonds in ClO1 (Scheme 1A). This result is in accordance with the reported mechanism for the response of cyanine dyes towards HClO.²³ In order to study the effects of different functional groups, we installed long (*n*-octadecyl alkane, C₁₈H₃₇) and short (*n*-butyl, C₄H₉) lipid chains. Meanwhile, we incorporated diverse amino groups including 2[[2-(dimethylamino)ethyl]methylamino]-ethyl groups (ClO1), 3-(dimethylamino)-propyl groups (ClO2 and ClO6), propyl-trimethylammonium groups (ClO3), and hexahydro-1H-azepine-1-ethyl (ClO4). ClO5 was synthesized as a control compound without amino groups.

In order to study the sensing ability of ClO1–ClO6 towards HClO, we first performed a spectral study in solution with serial concentrations of HClO. Briefly, we investigated the absorption and emission spectra of ClO1–ClO6 in phosphate buffered saline (PBS) by using a NaClO solution as the HClO source. Upon titration with NaClO, ClO1 displayed a significant decrease in the absorption peak at 638 nm and a gradual increase in the absorption peak at 540 nm (Fig. S2†).



Meanwhile, we observed an evident decrease in the peak at 760 nm and an increase in the peak at 605 nm in the emission spectrum of **C1O1** with increasing concentration of NaClO (Fig. 1A, excited at 530 nm). Consequently, **C1O1** exhibited a dramatic fluorescence ratio (I_{605}/I_{760}) enhancement from 0.1 to 6.9 in a NaClO concentration range of 0–14 μM (Fig. 1B). The detection limit of **C1O1** was calculated to be 0.1 μM (Fig. S3[†]). In order to investigate the effects of different reactive oxygen species (ROS) and reactive nitrogen species (RNS) on **C1O1**, we performed a selectivity study. As shown in Fig. S4 and S5,[†] **C1O1** demonstrated a minimal absorption change at 638 nm and a minimal fluorescence change at 760 nm upon the addition of a wide variety of ROS/RNS, metal ions and amino acids, while an apparent decrease was seen after the addition of HClO. Therefore, the reactivity of **C1O1** towards HClO is much higher than that towards other ROS and RNS. Also, **C1O1** displayed a significant decrease in absorption at 638 nm and a decrease in

fluorescence at 760 nm upon the addition of NaClO in the presence of Fe^{2+} and H_2O_2 , but showed low reactivity with reduced glutathione (GSH) (Fig. S4 and S5[†]). Yet, local concentrations of these analytes may be different in both cells and tissues. In addition, we found that **C1O2**, **C1O4** and **C1O6** showed similar patterns of changes towards NaClO in both the absorption and emission spectra (Fig. S6, S8 and S10[†]). However, **C1O3** and **C1O5** exhibited strong fluorescence peaks at both 560 nm and 750 nm without the presence of NaClO, which makes them unsuitable for ratiometric fluorescence imaging (Fig. S7 and S9[†]). Therefore, **C1O1**, **C1O2**, **C1O4** and **C1O6** were selected for cell imaging studies.

Next, we applied **C1O1**, **C1O2**, **C1O4** and **C1O6** to detect exogenous HClO (NaClO solution) in live A549 cells (a human lung adenocarcinoma cell line). We found that these probes were able to stain A549 cells (Fig. 2 and S11–S13[†]). Consistent with the spectral study in solution, **C1O1** showed weak

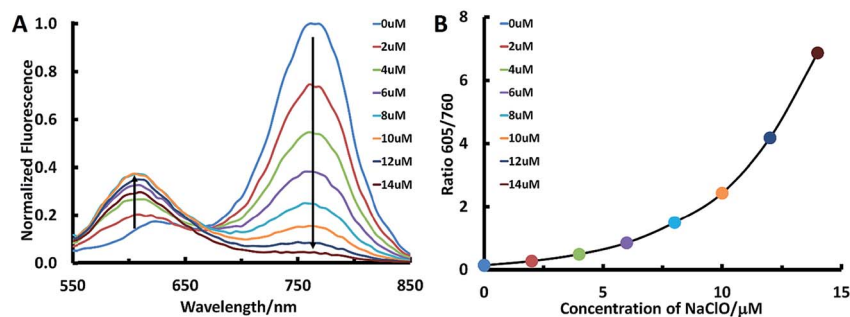


Fig. 1 (A) Emission spectra of **C1O1** (5 μM) upon treatment with various concentrations of NaClO (0–14 μM); (B) fluorescence ratio (I_{605}/I_{760}) of **C1O1** (5 μM) upon treatment with various concentrations of NaClO (0–14 μM).

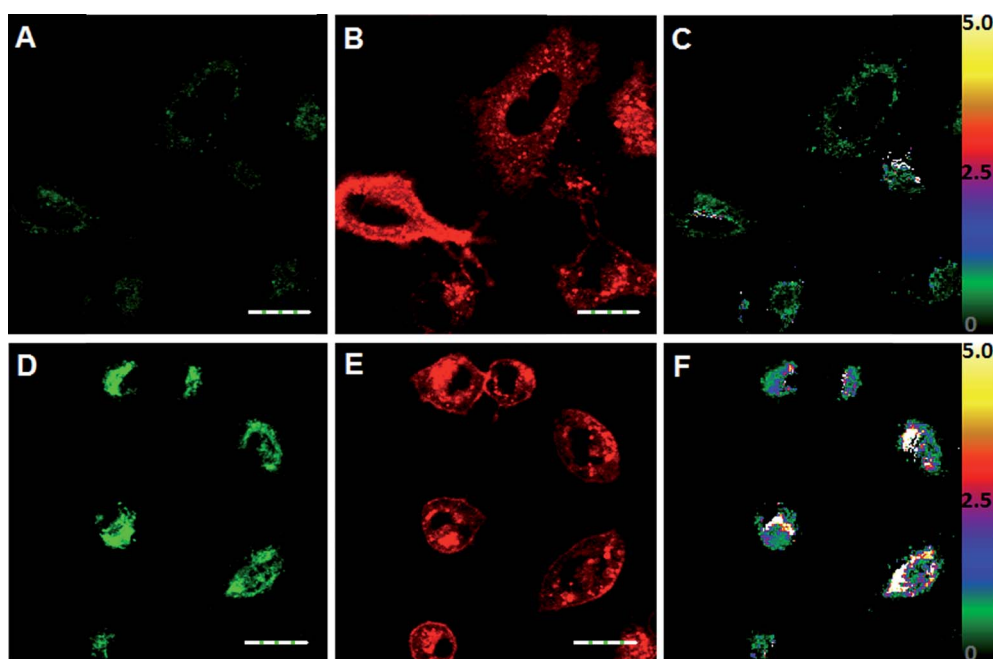


Fig. 2 Detection of exogenous HClO in A549 cells by **C1O1**. Cells were imaged with **C1O1** in the absence (A–C) or presence (D–F) of NaClO. (A) and (D) are green channels (560–660 nm); (B) and (E) are red channels (655–755 nm); (C) and (F) are the ratio images of the green/red channel. Scale bar = 20 μm .



fluorescence in the green channel (Fig. 2A, pseudo color green) and intense fluorescence in the red channel (Fig. 2B, pseudo color red) from the normal cell imaging. After treatment with NaClO, the cells displayed a remarkable enhancement in the fluorescence of the green channel (Fig. 2D) and a slight decrease in the fluorescence of the red channel (Fig. 2E). The ratio of the intensity in the two channels (green/red channel) increased dramatically from the baseline (Fig. 2C) to up to 5.0 (Fig. 2F), which indicates that **CIO1** possesses a robust ratiometric imaging property. **CIO6** displayed similar responses towards HClO in A549 cells to **CIO1** (Fig. S13[†]). **CIO2** and **CIO4** exhibited a much lower fluorescence enhancement in the green channel than **CIO1** and **CIO6** (Fig. S11 and S12[†]). Due to the high ratio enhancement in both the spectral study (0 to 6.9) and cell imaging (0 to 5.0), we selected **CIO1** for further *in vitro* and *in vivo* experiments.

In order to evaluate the ability of **CIO1** to detect *in situ* HClO production, we used lipopolysaccharides (LPS, endotoxins that cause the release of HClO in cells and animals⁴³) to induce endogenous HClO production in A549 cells. Briefly, cells were further incubated with or without LPS for 24 h after staining with **CIO1**. We observed an apparent fluorescence increase in the green channel of cells treated with LPS (Fig. 3D) as compared to the control group without the treatment with LPS (Fig. 3A). An enhancement of the fluorescence ratio (green/red channel) was detected from 0 (Fig. 3C) to 2.5 (Fig. 3F) upon treatment with LPS. These results indicated that **CIO1** was able to capture HClO molecules generated from LPS treated cells. Furthermore, in order to study the cytotoxicity of **CIO1**, an MTT assay was performed using a series of concentrations of **CIO1**.

As shown in Fig. S14,[†] the survival rate was higher than 90%, suggesting low cytotoxicity of **CIO1** at the tested concentrations (0.5–10 μ M).

Following the *in vitro* studies, we performed a bio-distribution study of **CIO1**–**CIO6** in C57BL/6 mice. Indocyanine green (**ICG**, an FDA approved cyanine for fluorescence imaging in the clinic⁴⁴) was used as a control. **CIO1**–**CIO6** and **ICG** were injected intravenously into mice. 1 h post injection, major organs (liver, lungs, spleen, kidneys, and heart) were harvested and imaged by using the IVIS fluorescence imaging system. **CIO1**–**CIO3** exhibited higher accumulation in the lungs than in other organs. **CIO4** and **CIO5** displayed higher distribution in both the spleen and lungs. **CIO6** and **ICG** showed a higher signal in the liver (Fig. 4). Based on the structural

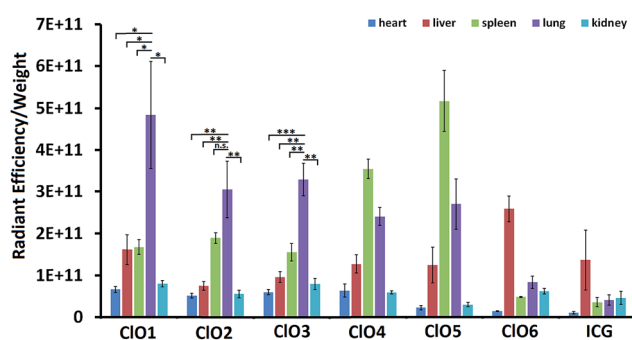


Fig. 4 The ratio of radiant efficiency to the organ weight of mice intravenously injected with **CIO1**–**CIO6** and **ICG**. ($n = 3$; * $P < 0.05$; ** $P < 0.01$; *** $P < 0.001$; n.s., $P > 0.05$; t test, double-tailed).



Fig. 3 Detection of endogenous HClO in A549 cells by **CIO1**. Cells were imaged with **CIO1** in the absence (A–C) or presence (D–F) of LPS. (A) and (D) are green channels (560–660 nm); (B) and (E) are red channels (655–755 nm); (C) and (F) are the ratio images of the green/red channel. Scale bar = 20 μ m.



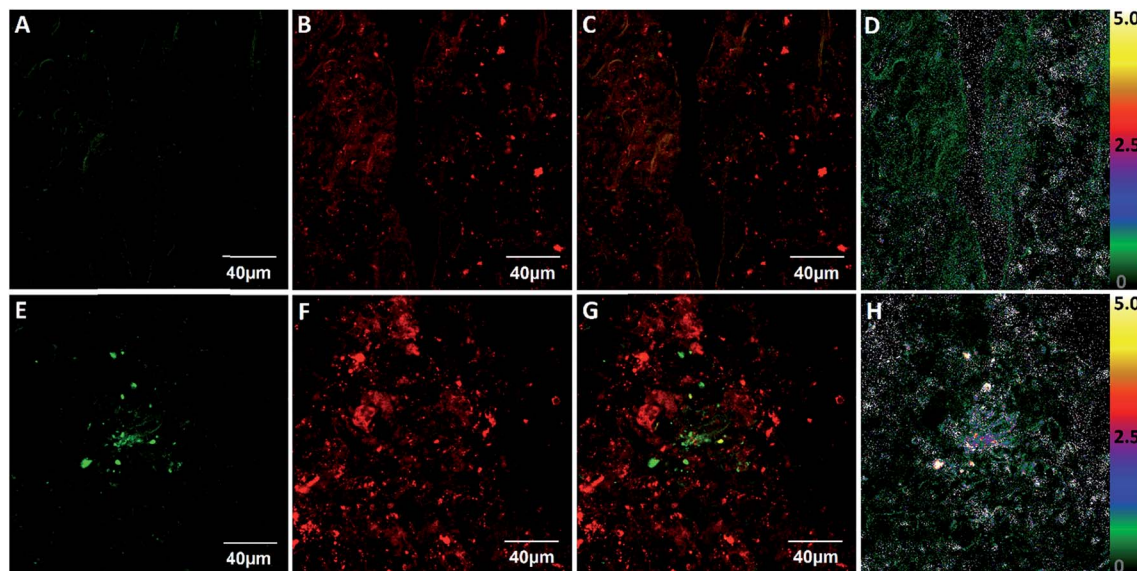


Fig. 5 Fluorescence imaging of the lung histology slides from mice intravenously injected with CIO1. (A–D) control mouse with intravenous injection of CIO1; (E–H) mouse treated with intranasal administration of LPS and intravenous injection of CIO1. (A) and (E) are green channels (560–660 nm); (B) and (F) are red channels (655–755 nm); (C) and (G) are overlay images of green and red channels; (D) and (H) are ratio images of green/red channels.

features of CIO1–CIO6 and their corresponding organ distribution, we found that a long lipid chain was favorable for lung accumulation. Also, amino groups were a critical factor for lung targeting (CIO1 vs. CIO4), and might be protonated in cells and produce positive charges. These results are consistent with previous reports that positive charges on nanoparticles affect their lung-targeting ability.^{40,42}

Lastly, we studied whether CIO1 was able to detect endogenous HClO at LPS-induced lung inflammation sites in mice. We first treated mice with LPS (intranasal administration) to induce acute lung inflammation. Then, we intravenously injected CIO1 into both untreated and LPS-treated mice. 1 h after the injection, the lungs of the mice were dissected and sectioned into ~100 μm slices and imaged under a confocal microscope. Strong fluorescence was observed in the red channel of both slices, which confirmed the accumulation of CIO1 in the lungs (Fig. 5B and F). Consistent with the *in vitro* results, many spots in the lungs treated with LPS produced a strong signal in the green channel (Fig. 5E), while minimal fluorescence was found in the green channel of the untreated lungs (Fig. 5A). The fluorescence ratio (green/red channel) at the inflammation sites was around 5.0 (Fig. 5H), which is much higher than that in the control lungs without inflammation (Fig. 5D).

Conclusions

In summary, we designed and synthesized a series of Cy7 based fluorescence ratiometric probes in order to detect HClO in the lungs. CIO1–CIO3 with long hydrophobic lipid chains and hydrophilic amino groups showed high accumulation in mouse lungs after intravenous injections. However, CIO4 with hexahydro-1H-azepine-1-ethanyl amino groups and CIO5 with *n*-

butyl (without amino groups) showed a higher uptake in the spleen than in other organs tested. CIO6 with short lipid chains displayed high distribution in the liver similar to ICG. These results indicated that both lipid chains and amino groups are important moieties for enabling the lung targeting effect of the probes. Moreover, an appropriate combination may dramatically increase the targeting specificity. Among these probes, CIO1, containing one *n*-octadecane chain and two 2-[[2-(dimethylamino)ethyl]methylamino]-ethyl groups, exhibited a sensitive fluorescence ratio response towards both exogenous and endogenous HClO in live cells. Based on the *in vivo* results, we demonstrated that CIO1 was able to capture LPS-induced HClO in the mouse lungs. These findings can be applied to design new probes for non-invasive and real-time monitoring of HClO *in vivo* in the future.

Conflicts of interest

There are no conflicts to declare.

Acknowledgements

Y. D. acknowledges the support from the Maximizing Investigators' Research Award 1R35GM119679 from the National Institute of General Medical Sciences as well as the start-up fund from the College of Pharmacy at The Ohio State University. All animal procedures were performed in accordance with the Guidelines for Care and Use of Laboratory Animals of The Ohio State University and experiments were approved by the Animal Ethics Committee of Institutional Animal Care and Use Committee (IACUC).



References

- 1 B. D'Autreaux and M. B. Toledano, *Nat. Rev. Mol. Cell Biol.*, 2007, **8**, 813–824.
- 2 T. Finkel and N. J. Holbrook, *Nature*, 2000, **408**, 239–247.
- 3 M. Valko, D. Leibfritz, J. Moncol, M. T. Cronin, M. Mazur and J. Telser, *Int. J. Biochem. Cell Biol.*, 2007, **39**, 44–84.
- 4 C. C. Winterbourn, *Nat. Chem. Biol.*, 2008, **4**, 278–286.
- 5 P. Zhang, H. Wang, Y. Hong, M. Yu, R. Zeng, Y. Long and J. Chen, *Biosens. Bioelectron.*, 2018, **99**, 318–324.
- 6 H. Xiao, J. Li, J. Zhao, G. Yin, Y. Quan, J. Wang and R. Wang, *J. Mater. Chem. B*, 2015, **3**, 1633–1638.
- 7 P. Zhang, Y. Tian, H. Liu, J. Ren, H. Wang, R. Zeng, Y. Long and J. Chen, *Chem. Commun.*, 2018, **54**, 7231–7234.
- 8 P. Zhang, X. F. Jiang, X. Nie, Y. Huang, F. Zeng, X. Xia and S. Wu, *Biomaterials*, 2016, **80**, 46–56.
- 9 P. Zhang, X. Nie, M. Gao, F. Zeng, A. Qin, S. Wu and B. Z. Tang, *Mater. Chem. Front.*, 2017, **1**, 838–845.
- 10 Y. Huang, P. Zhang, M. Gao, F. Zeng, A. Qin, S. Wu and B. Z. Tang, *Chem. Commun.*, 2016, **52**, 7288–7291.
- 11 C.-H. Sam and H.-K. Lu, *Journal of Dental Sciences*, 2009, **4**, 45–54.
- 12 C. C. Winterbourn, M. B. Hampton, J. H. Livesey and A. J. Kettle, *J. Biol. Chem.*, 2006, **281**, 39860–39869.
- 13 B. Kwaśny-Krochin, M. Bobek, E. Kontny, P. Gluszko, R. Biedroń, B. M. Chain, W. Maśliński and J. Marcinkiewicz, *Amino Acids*, 2002, **23**, 419–426.
- 14 M. Casciaro, E. Di Salvo, E. Pace, E. Ventura-Spagnolo, M. Navarra and S. Gangemi, *Immun. Ageing*, 2017, **14**, 21.
- 15 Y. W. Jun, S. Sarkar, S. Singha, Y. J. Reo, H. R. Kim, J.-J. Kim, Y.-T. Chang and K. H. Ahn, *Chem. Commun.*, 2017, **53**, 10800–10803.
- 16 L. Yuan, L. Wang, B. K. Agrawalla, S.-J. Park, H. Zhu, B. Sivaraman, J. Peng, Q.-H. Xu and Y.-T. Chang, *J. Am. Chem. Soc.*, 2015, **137**, 5930–5938.
- 17 H. Li, L. Guan, X. Zhang, H. Yu, D. Huang, M. Sun and S. Wang, *Talanta*, 2016, **161**, 592–598.
- 18 S.-k. Yao and Y. Qian, *Sens. Actuators, B*, 2017, **252**, 877–885.
- 19 L.-L. Xi, X.-F. Guo, C.-L. Wang, W.-L. Wu, M.-F. Huang, J.-Y. Miao and B.-X. Zhao, *Sens. Actuators, B*, 2018, **255**, 666–671.
- 20 Y. L. Pak, S. J. Park, D. Wu, B. Cheon, H. M. Kim, J. Bouffard and J. Yoon, *Angew. Chem., Int. Ed.*, 2018, **57**, 1567–1571.
- 21 P. Zhang, H. Wang, D. Zhang, X. Zeng, R. Zeng, L. Xiao, H. Tao, Y. Long, P. Yi and J. Chen, *Sens. Actuators, B*, 2018, **255**, 2223–2231.
- 22 B. Zhang, X. Yang, R. Zhang, Y. Liu, X. Ren, M. Xian, Y. Ye and Y. Zhao, *Anal. Chem.*, 2017, **89**, 10384–10390.
- 23 Z. Lou, P. Li, P. Song and K. Han, *Analyst*, 2013, **138**, 6291–6295.
- 24 L. Wu, I. C. Wu, C. C. DuFort, M. A. Carlson, X. Wu, L. Chen, C.-T. Kuo, Y. Qin, J. Yu, S. R. Hingorani and D. T. Chiu, *J. Am. Chem. Soc.*, 2017, **139**, 6911–6918.
- 25 M. Ren, B. Deng, K. Zhou, X. Kong, J.-Y. Wang, G. Xu and W. Lin, *J. Mater. Chem. B*, 2016, **4**, 4739–4745.
- 26 H. Zhu, J. Fan, J. Wang, H. Mu and X. Peng, *J. Am. Chem. Soc.*, 2014, **136**, 12820–12823.
- 27 L. Cao, R. Zhang, W. Zhang, Z. Du, C. Liu, Z. Ye, B. Song and J. Yuan, *Biomaterials*, 2015, **68**, 21–31.
- 28 J. Fan, H. Mu, H. Zhu, J. Wang and X. Peng, *Analyst*, 2015, **140**, 4594–4598.
- 29 Z. Qu, J. Ding, M. Zhao and P. Li, *J. Photochem. Photobiol., A*, 2015, **299**, 1–8.
- 30 C. Liu, X. Jiao, S. He, L. Zhao and X. Zeng, *Talanta*, 2017, **174**, 234–242.
- 31 K. Li, J.-T. Hou, J. Yang and X.-Q. Yu, *Chem. Commun.*, 2017, **53**, 5539–5541.
- 32 B. Zhu, L. Wu, M. Zhang, Y. Wang, C. Liu, Z. Wang, Q. Duan and P. Jia, *Biosens. Bioelectron.*, 2018, **107**, 218–223.
- 33 B. Zhu, L. Wu, M. Zhang, Y. Wang, Z. Zhao, Z. Wang, Q. Duan, P. Jia and C. Liu, *Sens. Actuators, B*, 2018, **263**, 103–108.
- 34 Y. Wang, L. Wu, C. Liu, B. Guo, B. Zhu, Z. Wang, Q. Duan, Z. Ma and X. Zhang, *J. Mater. Chem. B*, 2017, **5**, 3377–3382.
- 35 Z. Mao, M. Ye, W. Hu, X. Ye, Y. Wang, H. Zhang, C. Li and Z. Liu, *Chem. Sci.*, 2018, **9**, 6035–6040.
- 36 J. Peng, A. Samanta, X. Zeng, S. Han, L. Wang, D. Su, D. T. B. Loong, N.-Y. Kang, S.-J. Park, A. H. All, W. Jiang, L. Yuan, X. Liu and Y.-T. Chang, *Angew. Chem., Int. Ed.*, 2017, **56**, 4165–4169.
- 37 X. Jia, Q. Chen, Y. Yang, Y. Tang, R. Wang, Y. Xu, W. Zhu and X. Qian, *J. Am. Chem. Soc.*, 2016, **138**, 10778–10781.
- 38 D. Oshiki, H. Kojima, T. Terai, M. Arita, K. Hanaoka, Y. Urano and T. Nagano, *J. Am. Chem. Soc.*, 2010, **132**, 2795–2801.
- 39 E. R. Lee, J. Marshall, C. S. Siegel, C. Jiang, N. S. Yew, M. R. Nichols, J. B. Nietupski, R. J. Ziegler, M. B. Lane, K. X. Wang, N. C. Wan, R. K. Scheule, D. J. Harris, A. E. Smith and S. H. Cheng, *Hum. Gene Ther.*, 1996, **7**, 1701–1717.
- 40 R. Stribling, E. Brunette, D. Liggitt, K. Gaensler and R. Debs, *Proc. Natl. Acad. Sci. U. S. A.*, 1992, **89**, 11277–11281.
- 41 S. Azarmi, W. H. Roa and R. Löbenberg, *Adv. Drug Delivery Rev.*, 2008, **60**, 863–875.
- 42 O. F. Khan, E. W. Zaia, S. Jhunjhunwala, W. Xue, W. Cai, D. S. Yun, C. M. Barnes, J. E. Dahlman, Y. Dong, J. M. Pelet, M. J. Webber, J. K. Tsosie, T. E. Jacks, R. Langer and D. G. Anderson, *Nano Lett.*, 2015, **15**, 3008–3016.
- 43 C.-Y. Chuang, T.-L. Chen, Y.-G. Cherng, Y.-T. Tai, T.-G. Chen and R.-M. Chen, *Arch. Toxicol.*, 2011, **85**, 209–218.
- 44 G. Liberale, P. Bourgeois, D. Larsimont, M. Moreau, V. Donckier and T. Ishizawa, *Eur. J. Surg. Oncol.*, 2017, **43**, 1656–1667.

